AUTOMATIC CHARACTERIZATION OF SPIRAL AND ELLIPTICAL GALAXIES FROM DIGITAL IMAGES

J. A. García, R. Molina and N. Pérez de la Blanca
Departamento de Ciencias de la Computación e I.A.
Universidad de Granada. 18071 Granada. Spain.

Abstract

In this paper we describe the application of pattern recognition techniques to the astronomical problem of the automatic characterization of galaxies. The characterization problem is reduced to the study of the boundary of a region obtained from a segmentation process on the digital image. We show that there is enough information to characterize an elliptical or spiral galaxy from the information on the boundary of this region. This boundary exhibits deformations due to the arms on spiral galaxies, but shows a nearly elliptical shape on elliptical galaxies. Based on the information provided by this curve, we then study and compare three different galaxy characterization methods.

keywords and phrases: segmentation process, smoothing process,
image model, spiral and elliptical galaxies,
galaxy characterization, compactness, graph of curvature.
corresponding author: Rafael Molina
Departamento de Ciencias de la Computación e I.A.
Universidad de Granada. 18071 Granada. Spain.
e-mail : rms@robinson.ugr.es
fax : +34.58.243317

1 Introduction

Since William Herschel published his catalog of nebulae and star clusters in 1786, many astronomers have proposed systems to classify galaxies from their morphological shapes, with the one created by Hubble being the most widely used system. In general terms, Hubble classifies the galaxies in three groups: ellipticals, spirals and irregulars (Sandage (1961)).

In this paper, an application of pattern recognition methods to Astronomy will be described. The problem we shall be dealing with is the automatic classification as spiral or elliptical of an object present in an astronomical image. To perform the characterization task (see figure 1), we shall extract morphological features determining elliptical or spiral shapes. Taking into account that the appearance of spiral arms is enough to characterize the galaxy as belonging to the family of spiral galaxies, we shall thus, reduce the automatic characterization problem to that of detecting the presence or absence of arms in an appropriate region in the galaxy. As we will show, this region will be obtained from a four class partition of the area where the object is, performed by a completely data-driven segmentation technique.

The images used in this study have been obtained by scanning over 50 pictures from Sandage (1961) at 300 dpi and 256 grey levels. It is obvious that the process of capturing, printing and scanning introduces noise and very high non-linear transformations on the grey level of the images. However, for our characterization process the quality of the images is good enough. We also assume that accidental combinations of galaxies do not exist in these images.

The paper is divided as follows. In section 2 we describe the segmentation process. In section 3 we present three methods to solve the characterization problem, the information provided by each one being different; and also the results obtained are discussed. The conclusions are presented in section 4.

2 The segmentation process

Our goal is to reduce the galaxy classification problem to the simpler problem of studying the deformations present on a closed contour obtained from a segmentation process of the

grey level image. In stage one, an initial segmentation of the image will be obtained by thresholding the image according to a simple criteria. In stage two, a final segmentation will be performed by smoothing the initial segmentation. The smoothing process will be carried out by modelling the images as realizations of Markov random fields.

2.1 Initial segmentation

The initial segmentation is obtained by statistical thresholding (e.g., Mardia and Hainsworth (1988)). We assume that our images can be segmented in a finite number of classes *class* i, $i = 1, \cdots, L$ with the grey level in each class following a Gaussian distribution with mean μ_i and variance σ_i^2. Let us denote by x_k the grey level at pixel $k \in I$, the set of image pixels, then we classify the pixel k in the *class* j if

$$j = \arg\min_i \left(\frac{1}{2} \frac{(x_k - \mu_i)^2}{\sigma_i^2} + \frac{1}{2} \log(2\pi\sigma_i^2) \right) \tag{1}$$

where we assume equal prior probability for each class. This allocation rule can be reformulated in terms of a set of threshold values (Mardia and Hainsworth (1988)). In our case, the number of classes and the population parameters μ_i, σ_i, $i = 1, \cdots, L$, are all unknown.

To determine the number of classes in this initial segmentation, we performed the following experiments. First we used only three different regions: (a) high grey-level value pixels defining the center, (b) medium grey-level value pixels defining the intermediate zones and (c) low grey-level value pixels defining the background. The resulting segmentations were too smooth and they did not contain enough information so as to decide on the presence or absence of arms. This led us to introduce a fourth class between classes (b) and (c). The competition between the four classes (three for the light inside the galaxy and one for the dark background) increases the quality of the segmentation, recovering the basic geometric structure of the regions. The fourth class is used to separate the internal and external pixels in arms into two different classes on a spiral galaxy. This produces a region within which spiral arms are successfully detected. Figure $2C$ shows the four classes segmentation by thresholding of the galaxy depicted in figure $2A$, where the pixels clearly inside galaxy arms have been assigned to the two more internal classes of the galaxy (in which the two highest grey-level labels can be observed), and the rest of the pixels have been classified as

belonging to the other two classes with the lowest grey-level labels. Therefore, the shape of the region obtained by the union of the two more internal classes of the galaxy, shows clearly the deformations which are produced by the galaxy arms. But when the original image, figure $2B$, contains an elliptical galaxy, this region shows a nearly elliptical shape and such deformations do not appear, (see figure $2D$). The features allowing successful detection of spiral ams in the galaxy shape, are the deformations of the boundary (see figures $3C$ and $3F$) which is obtained as the contour surrounding the union of the two more internal classes of the galaxy (see figures $3E$ and $3B$) obtained by segmentation (from figures $3D$ y $3B$, respectively).

In order to estimate the parameters defining each class, we fix training areas taking into account some properties of the classes. To define the training area for $class1$, $Tclass1$, and to estimate the location of the galaxy center, $Center$, we proceeds as follows. Let J be defined as

$$J = \{s \in I \ : \ s \in (A \ominus \lambda \cdot B)\}$$

where A denotes a binary version of the original image taking the mode of the grey levels as the thresholding value, B being a three by three square and $A \ominus \lambda B$ denoting λ successive erosions of A by the structuring element B, and λ being calculated as follows. Let k be the last iterative step before A erodes to an empty set, that is $k = \max\{l \mid (A \ominus lB) \neq \emptyset\}$ then we take $\lambda = \max(0, k-3)$. Then, the training region for $class$ 1 is defined by $Tclass1 = \{s \in I \mid x_s > \eta_1\}$ where $\eta_1 = \text{median}\{x_s, s \in J\}$, and the location of the galaxy center, ($Center$), is defined as the baricenter of such a region. Two points are worth mentioning. Firstly, here we assume that the center of the galaxy is inside the largest foreground patch of the binary image. Secondly, the method we have described to find a central region works well when A is not corrupted by salt and pepper noise. To remove such noise, a median filter could be applied before eroding.

To obtain the training area for $class$ 4, $Tclass4$, we proceed as follows. Since the background grey-level values of the galaxy are nearly equal to a low value, we define $Tclass4 = \{s \ : \ x_s \leq \eta_4\}$ where $\eta_4 = \text{median}\{\mu_\theta \ : \ \theta \in [0, 2\pi)\}$, $\mu_\theta = \min\{x_s \mid s \in r(Center, \theta)\}$, and $r(Center, \theta)$ denotes an inside-image segment that with the origin in $Center$, forms an angle θ with the horizontal axis.

A provisional allocation of pixels belonging to $I-(Tclass1 \cup Tclass4)$ to one of the other two training classes is performed by using a simple iterative thresholding method (Mardia and Hainsworth (1988)).

Having estimated the parameters associated to each one of the four classes from the training areas, equation (1) can be used to perform the initial segmentation by assigning each pixel to its most probable class.

2.2 Smoothing process

The thresholding method described in Section 2.1 has been found to produce final classifications which suffer from blobs of noise (see figures $2B$ and $2D$). To clean the initial segmentation, we use a smoothing procedure assigning each pixel to one of the allowed classes based on some local processing on the neighborhood of the pixel. To do this, we will consider the grey level and segmented images as realizations of different but related Markov random fields (MRF), where once the prior distribution on the images and the likelihood are fixed, we will calculate the posterior distribution using the Bayes's rule. The image taking the maximum of the posterior distribution (MAP) will be considered as our final segmentation. In this context, the initial segmentation is used as the starting point to find the MAP estimator. The variance values associated to each class in the initial segmentation will be kept fix in this smoothing process.

2.2.1 Image model

Now we will present a description of the assumed image model. Let $X = \{X_s \mid s \in I\}$ be the grey-level image, for the segmentation process we assume

$$X_s = X_s^E + \varepsilon_s \ , \quad s \in I \tag{2}$$

where X_s^E denotes the label of the pixel s, with $X_s^E \in \{\mu_1, \mu_2, \mu_3, \mu_4\}$, and $\{\varepsilon_s\}$ the noise random field consisting of independent Gaussian random variables with mean zero and variance $\sigma^2_{X_s^E}$, in other words

$$\varepsilon_s \rightsquigarrow N(0, \sigma^2_{X_s^E}) \ , \quad \text{with} \ \ \sigma^2_{X_s^E} \in \left\{\sigma_1^2, \sigma_2^2, \sigma_3^2, \sigma_4^2\right\}$$

σ_i^2 being the variance of *class* i. Segmentation in this context produces a map of $\{X_s^E\}$ from $\{X_s\}$.

A Markov random field (MRF) with respect to a second-order neighborhood system can be specified by giving the distribution at each pixel conditional on the labels of its neighbours (see Geman (1990), for details). For our model, the functional form of this conditional distribution is

$$P\left(x_s^E = c \mid x_t^E, t \neq s\right) \propto \exp\left\{-\beta \sum_{t \text{ neighbour of } s} \phi\left(c - x_t^E\right)\right\} \tag{3}$$

for a positive constant β and where $\phi(u) = 1 - \frac{2}{1+(u/\delta)^2}$, being δ a scale factor.

The estimation of β and δ is not an easy task. Here we have followed the approach developed in Molina *et al* (1992) where the prior is approximated by a suitable conditional autorregressive model. The values obtained for our images were $\beta = 2.5$ and $\delta = 20$.

Once we have fixed a model defining a prior distribution on X^E, we compute the posterior distribution by

$$P(X^E \mid X) \propto \exp\left\{-\beta \sum_{(r,t)} \phi\left(x_r^E - x_t^E\right) - \frac{1}{2} \sum_r \frac{\left(x_r - x_r^E\right)^2}{\sigma^2_{x_r^E}}\right\} \tag{4}$$

where (r, t) are neighbour pixels, and we maximize it to obtain the MAP. Figure 3 shows the results of applying this method to our image examples.

Before leaving this section, it is important to note that a more realistic image formation model than (2) would have to take into account the blurring process. However, for the images we have being dealing with, the blurring matrix is symmetric and shift invariant, and so the maximization of (4) with respect to the labels including the blurring matrix, would be more computationally demanding and would produce the same segmentation but for a displacement of the boundaries between regions.

3 The characterization methods

Once the segmentation has been performed, and to characterize spiral and elliptical galaxies, we use three different techniques based on the information provided by the curve C, which

containing the previously defined center of the galaxy, $Center$, defines the boundary between $Class$ 2 and 3 regions. This curve exhibits deformations due to the arms on spiral galaxies, but shows nearly elliptical shape on elliptical galaxies (see figures $3E$ and $3F$).

3.1 Characterization using a compactness descriptor

A very well known descriptor defining the compactness of a closed shape (Pettijohn (1970)) is

$$\rho = \frac{1}{4\pi}\frac{\text{perimeter}^2}{\text{area}} \tag{5}$$

The main drawback of this descriptor is that it confuses roundness and circularity (see Serra (1982)). But as we will show, this objection is not critical in our case.

This dimensionless quantity is insensitive to scale changes. With exception of the errors introduced by rotation on rectangular lattices, this index is also insensitive to orientation, taking the minimum value for disk-shaped regions.

Let us denote by R_C the region enclosed by the curve C. Since the regions R_C obtained on elliptical galaxies are nearly ellipticals, we would obtain a characterization procedure if the ρ values for regions R_C on elliptical galaxies, were significantly lower than the ρ values for regions R_C on spiral galaxies.

Our criterium to perform the classification of galaxies as spiral or elliptical using the compactness value ρ for R_C is the following: the object in the astronomical image is classified as

$$\left\{ \begin{array}{ll} \text{an elliptical galaxy} & \text{if } \mid \rho - \overline{\rho_E} \mid = \min\{\mid \rho - \overline{\rho_E} \mid, \mid \rho - \overline{\rho_S} \mid\} \\ \text{a spiral galaxy} & \text{if } \mid \rho - \overline{\rho_S} \mid = \min\{\mid \rho - \overline{\rho_E} \mid, \mid \rho - \overline{\rho_S} \mid\} \end{array} \right\}$$

denoting $\overline{\rho_E} = \sum_{t=1}^{n_E} \frac{\rho_t^E}{n_E}$, with n_E being the number of elliptical galaxies in the sample ($n_E = 25$), and where ρ_t^E denotes the value of the compactness calculated on the corresponding elliptical galaxy, and denoting $\overline{\rho_S} = \sum_{t=1}^{n_S} \frac{\rho_t^S}{n_S}$, with n_S being the number of spiral galaxies in the sample ($n_S = 25$), and where ρ_t^S denotes the value of the compactness calculated on the corresponding spiral galaxy.

Let us now discuss the quality of this classification method. If we define (using the estimates of means and standard deviations on table 1):

$$R = \overline{\rho_S} - \overline{\rho_E} = 3.161$$

and $\sigma = \max\{\sigma(\rho^E), \sigma(\rho^S)\} = 0.293$, where $\sigma(\cdot)$ stands for standard deviation; we have $\frac{R}{\sigma} = 10.78$. Therefore, the means of ρ^E and ρ^S are separated by approximately 10 times the maximum σ of the standard deviations. Furthermore, the results obtained by using all the scanned galaxies, 50, show that the maximum value of ρ for regions R_C on elliptical galaxies, is less than 2.5, while the minimum value of ρ for regions R_C on spiral galaxies, is greater than 3.75.

On the other hand, it could happen that the lower (respectively upper) tail of the distribution of ρ^S (resp. ρ^E) overlapped the upper (resp. lower) tail of ρ^E (resp. ρ^S). However, this event is extremely unlikely. By using Chebyshev's inequality and the estimates of the mean and standard deviation on table 1, we have

$$Prob\{\mid \rho^E - \overline{\rho_E} \mid \leq 5\sigma\} \leq 0.03$$

and

$$Prob\{\mid \rho^S - \overline{\rho_S} \mid \leq 5\sigma\} \leq 0.04$$

and so the possible overlapping has a negligible effect ($Prob \leq 0.07$).

3.2 Characterization of elliptical galaxies

Taking into account the nearly elliptical shape of C on elliptical galaxies, a second approach to characterize elliptical galaxies can be obtained by fitting an elliptical contour to C. In our case we have adopted a least square fit (see Sampson (1982)).

Let $C = \{p_i = (x_i, y_i) \mid i = 1, \cdots, n\}$ denote the set of points defining C. Let $E(a, b, \theta)$ be the ellipse fitted to C, with a, b being the major and minor axis respectively, θ being the angle between the major axis a and the horizontal line, and the position of the ellipse center, $Center$, defined as the baricenter of the class $Tclass1$ obtained in section 2.1. The distance $D(C, E)$ between the curve C and the ellipse E, is defined as

$$D(C, E) = \frac{area(R_C \cup R_E - R_C \cap R_E)}{area(R_C \cup R_E)}$$

R_E being the region enclosed by E and where $area(\cdot)$ denotes the area of the corresponding region, the bounds of the distance $D(C, E)$ are $0 \leq D(C, E) < 1$.

Our criterium of classification using the distance value D is the following: the object in the astronomical image is classified as

$$\left\{ \begin{array}{ll} \text{an elliptical galaxy} & \text{if } \mid D - \overline{D_E} \mid = \min\left\{ \mid D - \overline{D_E} \mid, \mid D - \overline{D_S} \mid \right\} \\ \text{a spiral galaxy} & \text{if } \mid D - \overline{D_S} \mid = \min\left\{ \mid D - \overline{D_E} \mid, \mid D - \overline{D_S} \mid \right\} \end{array} \right\}$$

denoting $\overline{D_E} = \sum_{t=1}^{n_E} \frac{D_t^E}{n_E}$, with n_E being the number of elliptical galaxies in the sample ($n_E = 25$), and where D_t^E denotes the value of the distance calculated on the corresponding elliptical galaxy, and denoting $\overline{D_S} = \sum_{t=1}^{n_S} \frac{D_t^S}{n_S}$, with n_S being the number of spiral galaxies in the sample ($n_S = 25$), and where D_t^S denotes the value of the distance calculated on the corresponding spiral galaxy.

The results obtained in our sample of scanned galaxies show that the maximum value of D on elliptical galaxies is less than 0.2, and the minimum value of D on spiral galaxies is greater than 0.4. Furthermore, the means of D^E and D^S are separated by approximately 10 times the maximum σ of the standard deviations, and by using Chebyshev's inequality and the estimates of the mean and standard deviation on table 2, we have

$$Prob\{\mid D^E - \overline{D_E} \mid \leq 5\sigma\} \leq 0.02$$

and

$$Prob\{\mid D^S - \overline{D_S} \mid \leq 5\sigma\} \leq 0.04$$

and so the possible overlapping for this second method also has a negligible effect ($Prob \leq 0.06$).

3.3 Characterization of Spiral galaxies

The final method we have studied to characterize the shape of a galaxy, uses the graph of the curvature values computed from the digital curve C. The continuous expression to calculate curvature values on each point of a parametric curve $\{(x(t), y(t) \mid t \in R)\}$ is

$$k = \frac{\dot{x}\ddot{y} - \dot{y}\ddot{x}}{(\dot{x}^2 + \dot{y}^2)^{\frac{3}{2}}} \tag{6}$$

where $(\dot{\ }), (\ddot{\ })$ denote first and second derivatives respectively. To apply this expression to our discrete contour C we must control the spatial quantization noise. To minor the noise,

we have estimated the Gaussian curvature at each point using a Gaussian filter to smooth the quantization noise (Mokhtarian and Mackworth (1986)).

When the contour C is extracted from spiral galaxies, the graph of the curvature values $K = \{k(i) \mid i = 1, \cdots, n\}$ shows strong oscillations (see figure 4). This behaviour is not present when we analyze curves from elliptical galaxies (see figure 5). Then, this property can be used to characterize spiral galaxies.

3.3.1 Fitting a theoretical pattern to the graph of curvature values

Let $C^{+}_{deformed}$ (respectively $C^{-}_{deformed}$) be a contour fragment (of the curve C), which is deformed due to the presence of a spiral arm with positive (resp. negative) curvature. Let

$$p_{+}(s) = \begin{cases} \phi_1 h(s,\sigma) & s \leq 0 \\ \phi_2 h(s,\sigma) & s > 0 \end{cases}$$

where ϕ_1, ϕ_2 are two positive real numbers, and

$$h(s,\sigma) = \frac{s}{\sigma^2}\frac{1}{\sqrt{2\pi}\sigma}\exp\left\{-\frac{s^2}{2\sigma^2}\right\}, \text{ and}$$

(see figure 6), and let $p_{-}(s) = -p_{+}(s)$.

The functions, $p_{+}(s), p_{-}(s)$, show around zero qualitative deformations similar to those produced on the graph of curvature values K by the presence of arms in spiral galaxies, and so they can be used as templates to match possible arm occurrences. Let $T = \{1, \cdots, n\}$ the set of indexes associated to the graph of curvature values, then the most likely positions of the pattern p_{+} (or p_{-}) in K, are the values $i \in T$ maximising the normalized cross-correlation between p_{+} (or p_{-}) and K

$$\frac{\sum_s k(s+i)p_{+}(s)}{(\sum k(s+i)^2 \sum p_{+}(s)^2)^{\frac{1}{2}}}. \tag{7}$$

In order to calculate the points maximizing (7) we proceed as follows. Let

$$\overline{k} = \frac{1}{|T|}\sum_{i\in T} k(i), \quad \text{and} \quad st^2 = \frac{1}{|T|}\sum_{t\in T}\left(k(i) - \overline{k}\right)^2,$$

then we define two subsets of local extremes in curvature K

$$K_{sup} = \{k(i) \in K \mid k(i) > \overline{k} + 3st, i \in T \text{ and local maximum }\}$$

and

$$K_{inf} = \{k(i) \in K \mid k(i) < \overline{k} - 3st, i \in T \text{ and local minimum } \}$$

Let Q be the ordered set of indexes $i \in T$ such that $k(i) \in K_{inf} \cup K_{sup}$. Let $P = \{(p,q) \in Q \times Q \mid q = \text{ next after } p \text{ in } Q, \text{ with } k(p) \in K_{inf}(resp.\ K_{sup}) \text{ and } k(q) \in K_{sup}(resp.\ K_{inf})\}$.

Then the set of points $i \in T$ on which we calculate the cross-correlation is given by

$$L = \left\{ i \in T \mid i = \left[\frac{(p+q)}{2}\right] \text{ , and } (p,q) \in P \right\}$$

The values for σ, ϕ_1, ϕ_2 are chosen as follows, $\sigma = 0.5 \cdot (q + n - p) \bmod n$ and ϕ_1, ϕ_2 are taken to fix the values of $p_+(\sigma)$ and $p_+(-\sigma)$ equal to $k(p) > 0$ and $k(q) < 0$ respectively. Similarly for $p_-()$ we fix $p_-(\sigma) = k(q) < 0$ and $p_-(-\sigma) = k(p) > 0$ to estimate ϕ_1, ϕ_2.

When the graph of curvature values K exhibits the pattern p_+ (or p_-), the minimum values of the normalized cross correlation are greater than 0.7, but when K does not exhibit the pattern p_+ (or p_-), the maximum values of the normalized cross correlation are lower than 0.3. These results have been obtained using our sample of images.

4 Conclusions

In this paper, we have shown that it is possible to automatically characterize the shape of galaxies from digital images. By segmenting and smoothing the images using statistical methods we have reduced the characterization problem to the study of the boundary of a region R_C obtained by a segmentation process on the original image. We have shown that to characterize an elliptical or spiral galaxy there is enough information on the boundary of this region. We have characterized spiral and elliptical galaxies using the following three approaches. Firstly, the characterization of elliptical galaxies has been performed by using the compactness for the region R_C. Secondly, elliptical galaxies have been characterized by using the distance between the boundary of R_C and a fitted elliptical model. Finally, we have used the graph of curvature values K computed on the boundary of R_C, to characterize the shape of the galaxy.

Although the three methods presented to characterize galaxies allow us to perform the classification task, the information provided by each one is different. The information pro-

vided by the values of the first criteria is only relevant if we wish to know a value of the galaxy compactness, but it does not provide us with complementary information on particular features of the shape. The second method is very convenient when applied to elliptical galaxies since for these cases we also obtain the length of the axes. However, information on important features to classify the galaxy such as number of arms and starting of the arms is provided by the third approach. Furthermore, thinking of numerical estimations of the length arms, the third approach is the only one able to provide a starting point. In a forthcoming paper we will present methods to obtain numerical estimations on galaxy features, in particular ellipticity on elliptical galaxies, number and length of the arms on spiral galaxies and bar presence or absence on spiral galaxies.

References

Geman, D. 1990. Random Fields and inverse problems in imaging. *Lectures Notes in Mathematics. École d'Eté de Probabilités de Saint-Flour XVIII-1988.* Springer–Verlag.

Mardia, K. V. and Hainsworth, T. J. (1988). A spatial thresholding method for image segmentation. *IEEE Trans. Pattern Analysis and Machine Intelligence*, PAMI-10, no. 6, 919-927.

Mokhtarian, F. and Mackworth, A. (1986). Scaled-based description and recognition of planar curves and two-dimensional shapes. *IEEE Trans. Pattern Analysis and Machine Intelligence*, PAMI-8, no. 1, pp. 34-43.

Molina, R. and Ripley, B. D. and Cortijo, F. J. (1992). On the Bayesian Deconvolution of the Planets. *Proceedings 11th IAPR International Conference on Pattern Recognition*, Vol III, 147-150.

Pettijohn, F. J. (1970). Sedimentary Rocks. *Harper and Row, New York.*

Sampson, R.D. (1982). Fitting Conic Section to Very Scattered Data: An Iterative Refinement of the Bookstein Algorithm. *Computer Graphics and Image Processing*, Vol. 18, pp. 97-108.

Sandage, A. (1961). The Hubble Atlas of Galaxies. *Carnegie Institution of Washington.*

Serra, J. (1982). Image Analysis and Mathematical Morphology. *Academic Press.*

FIGURE CAPTIONS

Figure 1. Classification Diagram.

Figure 2. A Original spiral galaxy. B Original elliptical galaxy. C Initial segmentation of A. D Initial segmentation of B.

Figure 3.A and D examples of spiral galaxies. B and E final segmentation of A and D respectively. C and F corresponding contours used in the classification process.

Figure 4.A and B Graphs of curvature obtained from figures $3C$ and $3F$ respectively.

Figure 5.A and B Graphs of curvature obtained from two elliptical galaxies.

Figure 6. Theoretical graph of curvature.

Class	Mean	Standard deviation
Spiral	4.635	± 0.293
Elliptical	1.474	± 0.262

Table 1: Mean and standard deviation for compactness

Class	Mean	Standard deviation
Spiral	0.53	± 0.04
Elliptical	0.11	± 0.03

Table 2: Mean and standard deviation for the distance D

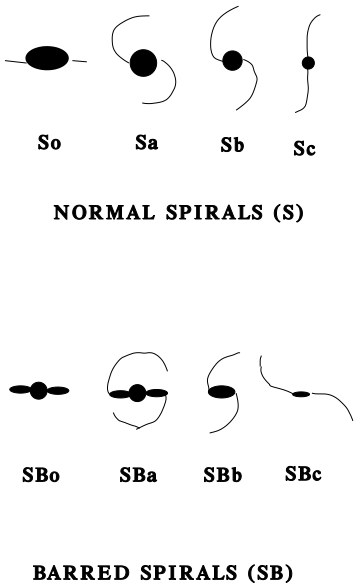

Figure 1:

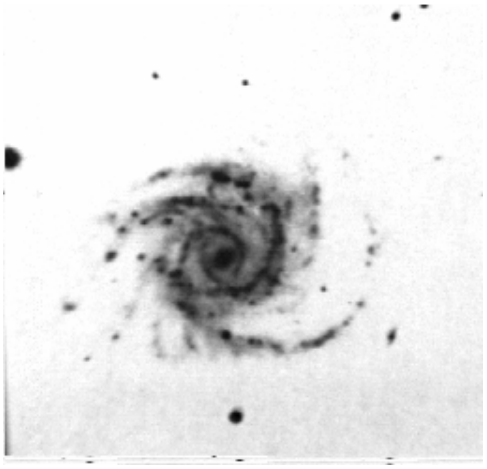

A

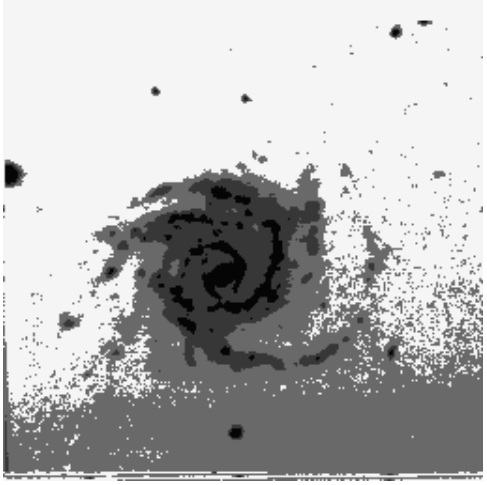

C

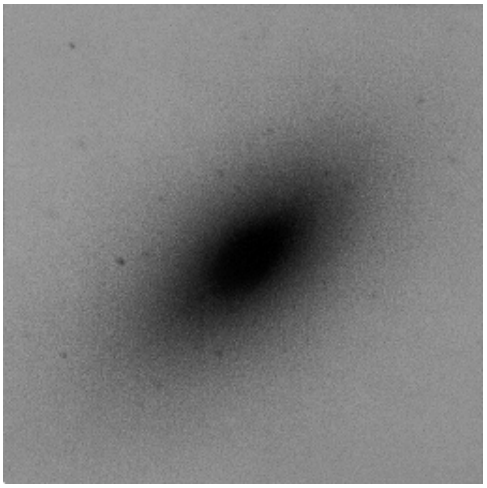

B

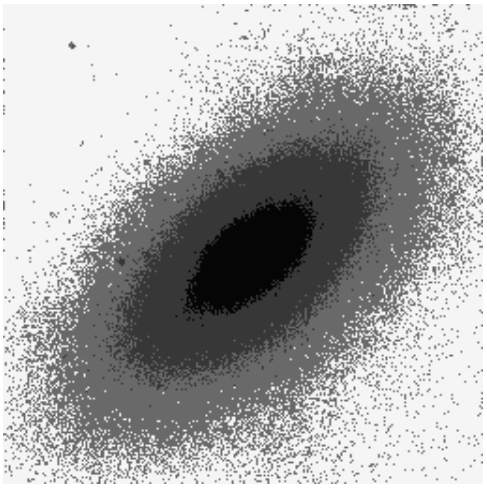

D

Figure 2:

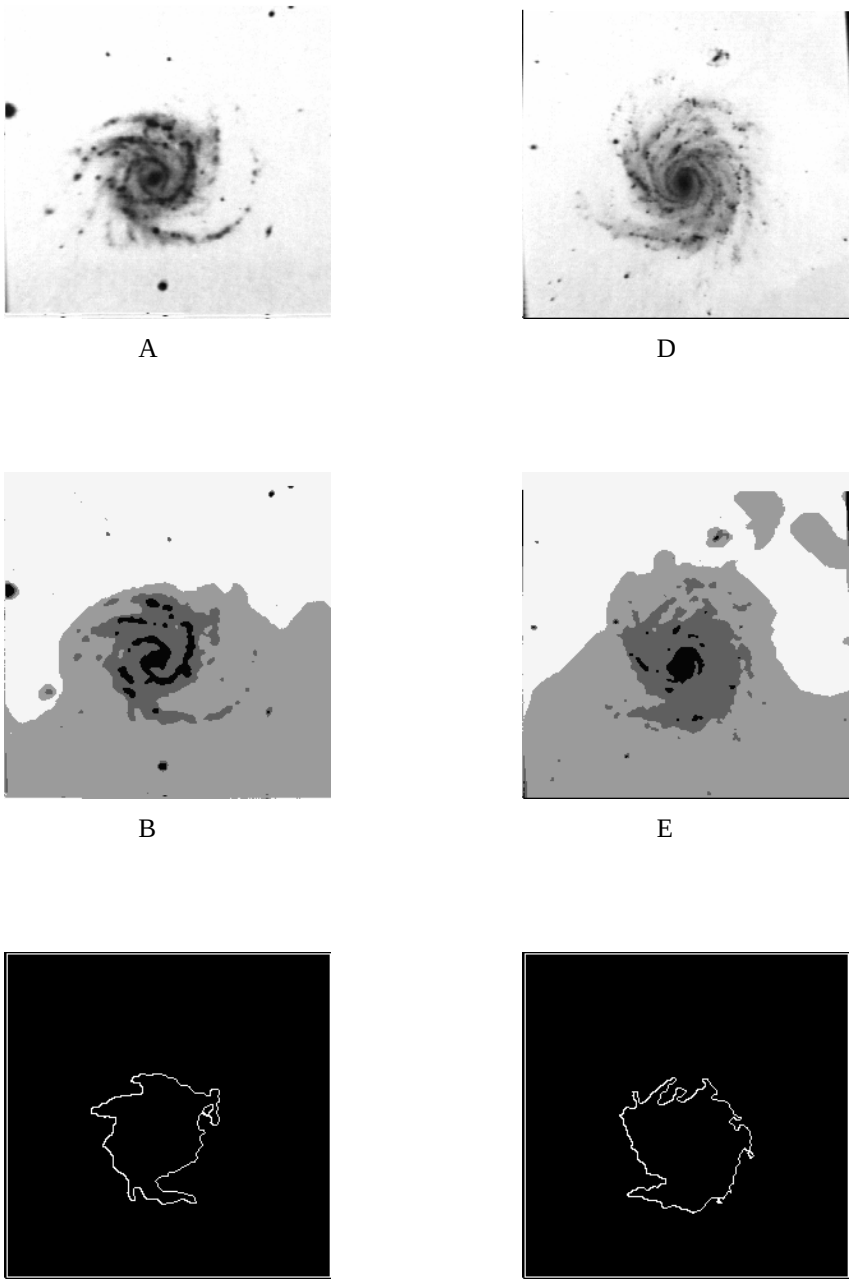

Figure 3:

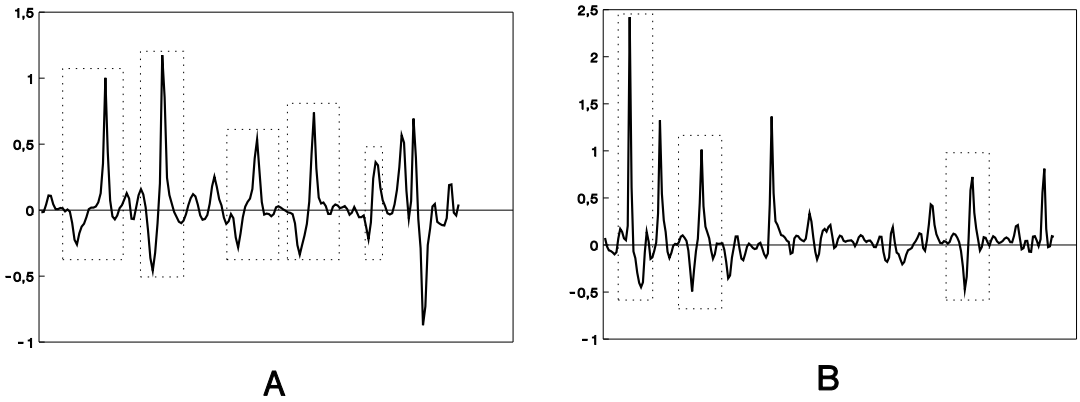

Figure 4:

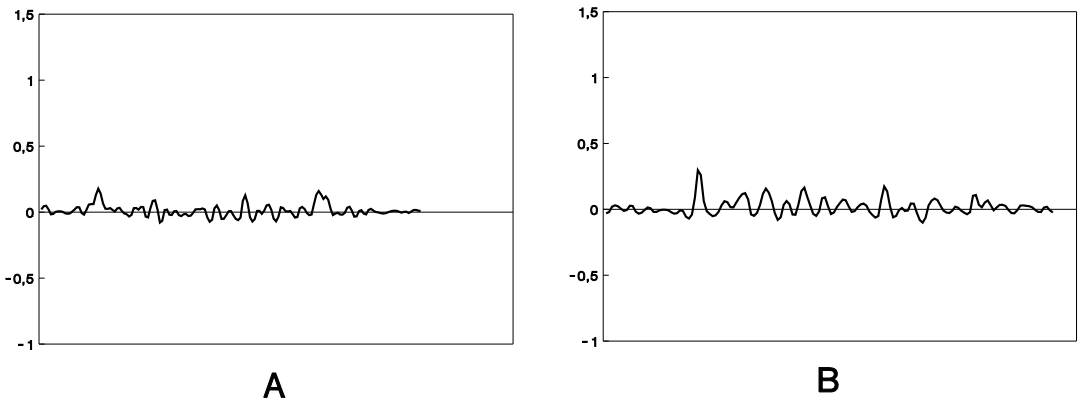

Figure 5:

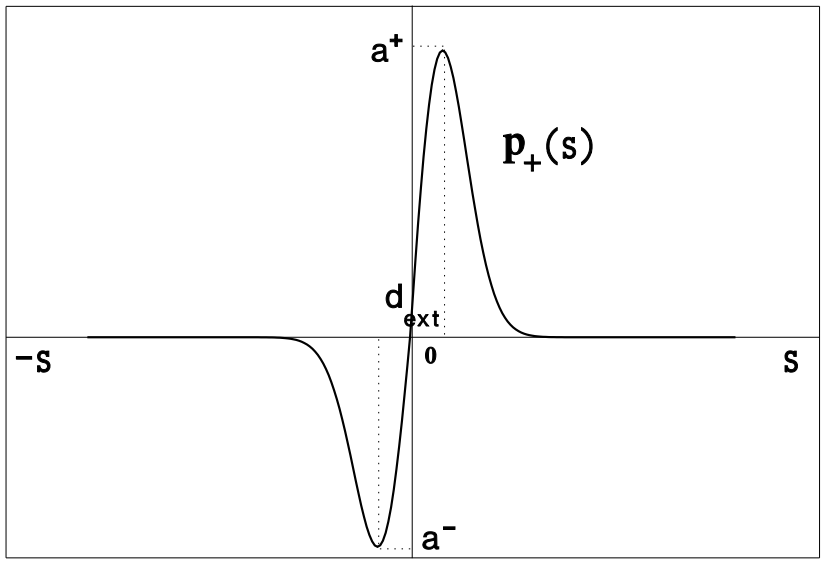

Figure 6: